Nonequilibrium and Equilibrium Shock Front Radiation Measurements

Surendra P. Sharma*
NASA Ames Research Center, Moffett Field, California 94035
and
Walter Gillespie†
Stanford University, Stanford, California 94305

The intensities of the radiation emitted behind a normal shock wave in nitrogen were measured in an electric-arc driven shock tube, at a shock velocity of 6.2 km/s. Both a time-resolved broadband radiation intensity measurement and a time-frozen spectral measurement were conducted. The time-frozen measurement was made by a 0.3-m spectrograph equipped with a 700-element linear diode array at the exit focal plane, which gave a spectral resolution of 0.3Å per element. By analyzing the second positive system of N_2 in the 3153–3159-Å wavelength region, the rotational and vibrational temperatures are determined in both the equilibrium and the nonequilibrium regions. The results are compared with similar data obtained by the AVCO-Everett Research Laboratory during the 1960s. The relaxation times and the temperature in the equilibrium region obtained in the present experiment agree with those of AVCO, but the vibrational and rotational temperatures in the nonequilibrium region are greatly different from the AVCO results. The measured rotational temperature seems to be in nonequilibrium, contradicting the two-temperature assumption of Park, but the measured vibrational temperature agrees with Park's model.

Introduction

As the aerospace community prepares for the design of the next-generation space transportation systems, it is becoming aware that more must be understood about the nature and effects of high-temperature real gas phenomena occurring in the flow around hypersonic vehicles. At hypersonic flight speeds, portions of the airflow around a vehicle are sufficiently hot to produce vibrational and rotational relaxation, dissociation, and ionization. Considerable effort has been expended in recent years to compute numerically the phenomena and their effects. Accuracy of such calculations is as yet to be verified: there are still many physical parameters that are unknown for high-temperature real gases. Thermochemical models describing the phenomena and the numerical algorithms used for the computation also contain many uncertainties. For these reasons, it becomes desirable to conduct an experiment. Such experiments can provide the needed physical constants and verify the validity of the thermochemical models and the computational algorithms used. A discussion of the types of experimental parameters needed to be measured has been discussed in Ref. 1.

The AVCO-Everett Research Laboratory, among others, studied the radiation phenomena behind a normal shock wave in a shock tube for both nitrogen[2–4] and air.[5] For nitrogen, the tests were conducted with an initial pressure of 1–10 Torr. The tested shock velocities varied up to 6.4 km/s. The radiation measurement was made by a simultaneous use of several monochromators with a spectral resolution on the order of 5 Å. The overall spectra were constructed by using the data from different runs in which the monochromators were set to different wavelengths. The radiation intensity characteristics of the N_2^+ first negative system were used to determine 1) the rotational temperature and 2) the vibrational temperatures; whereas the N_2 first positive data were used to deduce 1) the electronic excitation temperature, 2) variation of radiation intensities for several selected wavelength regions, 3) the time to reach the peak in the radiation intensity, and 4) the time to reach equilibrium. No serious efforts were made by AVCO to quantitatively explain the observed radiation characteristics. However, the experiments confirmed the presence of the radiation overshoot in the nonequilibrium region behind the shock wave. The data were then extrapolated to the flight environment to predict the radiative heat flux at the stagnation point of the re-entry vehicles. However, in the flight experiments of Fire and Apollo,[6] the measured radiative heat fluxes were considerably smaller than those deduced from the laboratory experiments, thereby showing that the simple extrapolation is not valid and that a more rigorous analysis is needed.

Using the latest information and innovations, Park[7] developed a two-temperature kinetic description to numerically reproduce the AVCO data. The theoretical model accounted for the diffusive nature of the vibrational relaxation and assumed that an average temperature $T_a = \sqrt{(T \times T_v)}$ controls the dissociation rates. According to his study, the coupling between vibrational relaxation and dissociation plays the key role in determining the thermochemical and radiative characteristics in the nonequilibrium region. Radiation behavior is sensitively affected by the vibration-dissociation phenomena, and, therefore, a theoretical model that reproduces the experimentally observed radiation characteristics can be trusted to predict thermochemical characteristics correctly also.[7] This model was successful in numerically reproducing most of the laboratory data, namely, the 1) rotational temperature, 2) electronic excitation temperature, 3) temporal variation of radiation intensities, 4) characteristic relaxation times, and 5) the ratio of nonequilibrium to equilibrium-radiative heat fluxes. However, the calculated vibrational temperature of the ground electronic state of N_2 did not agree at all with the measured

Presented as Paper 90-0139 at the AIAA 28th Aerospace Sciences Meeting, Reno, NV, Jan. 8–11, 1990; received Feb. 13, 1990; revision received Aug. 14, 1990; accepted for publication Aug. 16, 1990.

*Research Scientist, MIS 230-2. Associate Fellow AIAA.
†Graduate Student, Department of Aeronautics and Astronautics, Durand Bldg., Room 258. Student Member AIAA.

vibrational temperature of the B state of N_2^+, thereby casting a doubt on the model.[7] No other vibrational temperature measurements were available in the literature, which could check the accuracy of the AVCO data.

Sharma et al.[8] conducted at theoretical study of the coupled vibration-dissociation phenomena in nitrogen using a generalized Schwartz-Slawsky-Herzberg (SSH) approximation. The study showed that the coupled vibration-dissociation phenomenon is much more complex than is assumed in Park's model: the vibrational transition rates have a minimum in the middle of the vibrational ladder, which causes a bottleneck in the vibrational relaxation. The vibrational states above this bottleneck are likely to be in equilibrium with the dissociated state, whereas the lower vibrational states tend to follow the Landau-Teller theory. Thus, the vibrational relaxation behavior can not be described accurately by a single vibrational temperature, as assumed in Park's model.

In addition, since the 1960s, tremendous progress has been made in the detector technology, notably, the advent of multichannel analyzers. Although the measurements made by AVCO were quite an achievement in the early 1960s, today, better precision of the measurement and data reduction techniques can be applied. Also, the AVCO measurements relied on the repeatability of the same run conditions, taking a single point data at a time, to record a given spectrum. In addition, in deducing the vibrational and rotational temperatures, AVCO relied on the smeared band model, which is imprecise and inaccurate.

Therefore, it was felt that more precise spectral measurements and more precise data reduction are needed to accurately assess the existing models, thereby improving our ability to predict the thermochemical properties behind a shock wave. For this reason, a series of experiments in a nonequilibrium environment has been launched at NASA Ames Research Center with its electric-arc driven shock tube facility. This paper describes the first results from this series of experiments. In this experiment, we have repeated AVCO's nitrogen experiment with better instrumentation and a better data reduction technique. Specifically, the following improvements have been made:

1) A multichannel photoelectric sensor array placed at the exit focal plane of a spectrograph was used to record the full spectra in a single run, thereby eliminating the run-to-run jitter.

2) The same use of the sensor array provided a spectral resolution much higher than was attained by AVCO.

3) The spectral data were analyzed with a computer code that calculated the spectral characteristics line by line rather than with a smeared band model used by AVCO.

The data obtained were then compared with AVCO's data. Considerable difference was found between them, as will be elaborated later.

Experimental Technique

The electric arc-driven shock tube facility has existed at NASA Ames Research Center since the early 1960s. The operating characteristics of the facility charted during the initial phase of its operation are described in detail in a report by Reller,[9] and an updated version of the facility description has been discussed by the senior author.[10] For completeness, however, we will mention some of its relevant features. The shock tube driver is powered by a 1.2-MJ, 20-kV capacitor bank. With the use of various driver gas and driver configurations, the facility is capable of producing shock velocities in the range of 2–50 km/s.[1] The old 10-cm stainless steel driven tube was replaced by a new tube made of aluminum alloy (Fig. 1). The driven section is divided into two separate sections connected each to an independent vacuum system. The primary section, which is connected to the driver via the main diaphragm and contains the test section, is evacuated by a turbomolecular pump (Fig. 1). This vacuum system pumps the section down to a vacuum of 6.0×10^{-6} Torr. The secondary vacuum system serves the remainder of the driven tube and the dump tank. A thin secondary diaphragm separates the two vacuum systems.

Stations B, C, D, G, and H (Fig. 1) are equipped with an ionization probe that detects the shock arrival. By knowing the distance traveled and the respective time interval, the local shock velocity is computed. A highly sensitive photomultiplier tube (PMT) located at station A is used to detect the opening of the main diaphragm. Another PMT located at station E connected to a pulse trigger amplifier is used to generate a trigger pulse to gate various oscilloscopes and electronics. A broadband 1P28 PMT, with a 2500–6500-Å spectral response and 20-ns rise and fall time is used, in lieu of radiometer, to record the broadband emission radiation from the driven and driver gases as they pass through the test section (station F, Fig. 1).

A typical radiation from the radiometer PMT is shown in Fig. 2. The first sharp spike occurs soon after the shock arrives and is due to the nonequilibrium radiation from the compressed test gas. In about 200 ns (see photograph inset), the radiation starts to decrease and very quickly achieves an equilibrium value. The radiation from the driver gas follows after that with a distinct mark showing the interface between the two.

From the PMT traces, such as that shown in Fig. 2, the two characteristic relaxation distances, namely, the distance to the

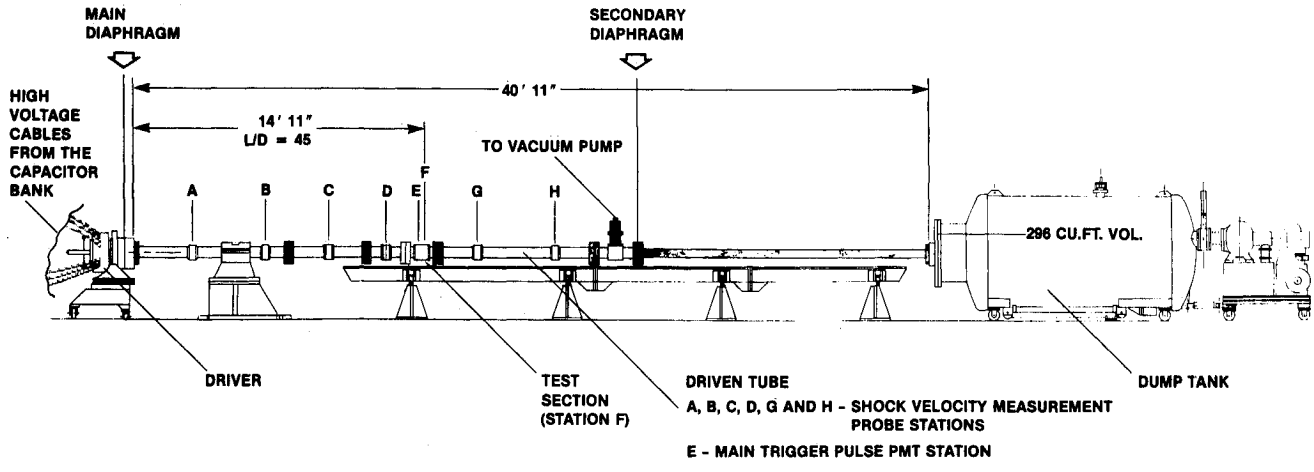

Fig. 1 Electric-arc driven shock tube facility.

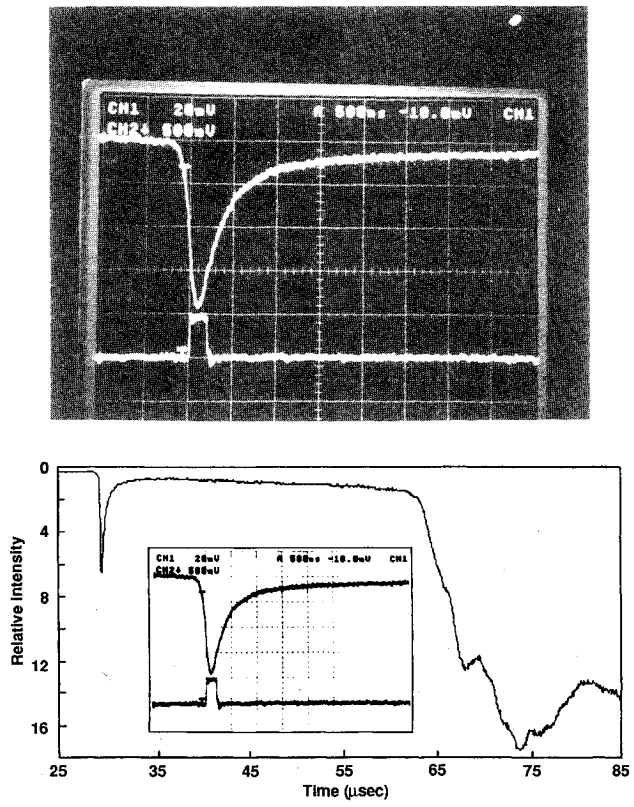

Fig. 2 Typical signal trace of the 1P28 PMT located at station F (test section). The inset photograph is the expanded view (500 ns/div) of the nonequilibrium radiation peak. Also shown in this photograph is the gate pulse sent out to the diode array image intensifier when the nonequilibrium radiation spectrum is recorded.

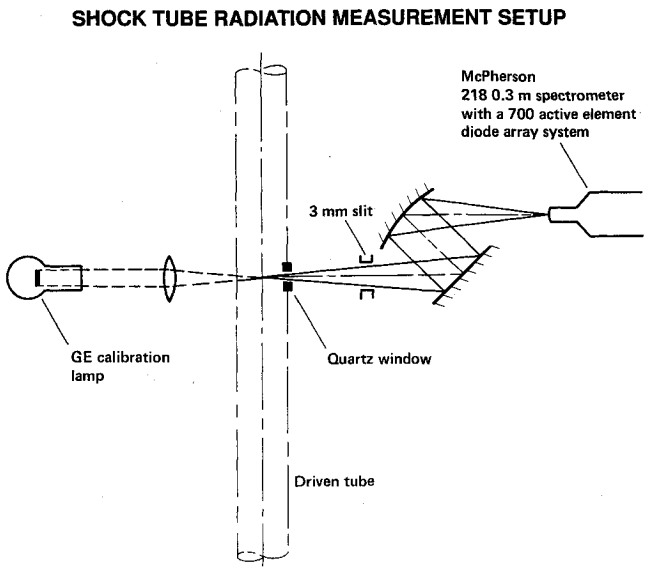

Fig. 3 Schematic of the collection optics arrangement for the diode array system.

peak radiation point and the distance to the equilibration point, are determined, as was done in the work of AVCO. The signal from one of these PMT is also used to trigger the multichannel spectrum analyzer system. The multichannel analyzer system, which is used to record the emission spectra, consists of 1) a 1024-element diode array system, 2) a 17.5-mm image intensifier, and 3) a system controller. The system controller clears the charge on the diode array before the run, sends high voltage gate signals to the image intensifier, reads the data from each of the diode elements after the exposure, and, then, sends the read data to the computer memory. Because of the smaller size of the image intensifier, compared to the diode array size, only 700 diode elements are considered active.

The diode array is mounted at the exit focal plane of a McPherson model 218 0.3-m spectrograph with a $f/5.3$ internal optics. The f number of the collection optics, shown in Fig. 3, is matched to that of the spectrograph. A 3-mm-wide slit, placed at a distance of 15 cm from the center of the driven tube, acts as the limiting aperture. A GE type 30A/T24/13 tungsten ribbon lamp is used to calibrate the diode array system for absolute measurements (Fig. 3). This GE lamp itself has been calibrated against the National Bureau of Standards (NBS) certified calibration standard as specified in the NBS Standard Reference Q-30 EPT 1342 by Epply Laboratories, Inc., Newport, RI. The width of the entrance slit for the spectrograph was kept at 60 μm throughout the measurements as well as during the calibration. Since the calibration was done by using the same optics, with an exception of a focusing lens (Fig. 3), ambiguities about the slit width accuracy, optics calibration, and image magnification correction were absent. The depth of the optical field was experimentally measured and, as shown in Fig. 4, was very uniform throughout the tube diameter. The shock velocity from run to run was repeatable within 2% of deviation, as seen from the plot shown in Fig. 5.

Results

Before recording the actual data, the quality of the test was verified. Spectra emitted by the driver gas and by the uncompressed and cold driven gas were recorded and are shown in Figs. 6 and 7, respectively. As expected, the driver gas spectrum shows lines primarily due to He and Al. The spectrum of the cold uncompressed driven gas was taken at 5 μs before the arrival of the shock and shows very little noise (Fig. 7), which may have been caused due to the instrument noise or due to the reflections in the shock tube.

In order to record the overall spectra of the equilibrium region, the spectrograph was equipped with a 1200-mm grating, and the diode array system was triggered at about 2.5–3.0 μs after the peak of the nonequilibrium radiation appeared on the radiometer PMT signal trace (Fig. 2). Since the signal levels were relatively low, the image intensifier was gated for 2.5 μs. The equilibrium spectra covering the 3050–4300-Å range were recorded in four runs. Each run covered approximately 378 Å in the wavelength range with a spectral resolution of 0.54 Å per element. The composite spectrum from these four runs is shown in Fig. 8. The shock velocities in these runs varied about 1% on the average. Since the absolute radiation intensities are a very strong function of the shock speed, the 1% difference in shock speed is accounted for in the data reduction. As seen from the figure, the spectrum is dominated by the N_2^+ bands even at these low-level ionizations. Some CN violet radiation is seen at around 3883 Å. Radiation from the N_2 second positive (2^+) band system is also seen in the ultraviolet range. The (1,0) and 2,1) band systems of the $N_2(2^+)$ system near 3159 Å is unobstructed and is free from other band systems.

The overall spectrum in the nonequilibrium region was recorded by triggering the same system about 40–50 ns before the onset of the peak radiation, with the intensifier gated to an opening of about 200 ns. It would have been desirable to reduce the gating time to capture the radiation from the very top of the peak, but in doing so, the signal-to-noise ratio deteriorates. In comparing the measured data with the calculated spectra, this fact was accounted for by averaging the calculated spectra over a range. The nonequilibrium spectrum was taken also in four runs. Figure 9 shows the composite of the spectra in the nonequilibrium region taken in four separate runs. As seen here, the nonequilibrium radiation is stronger

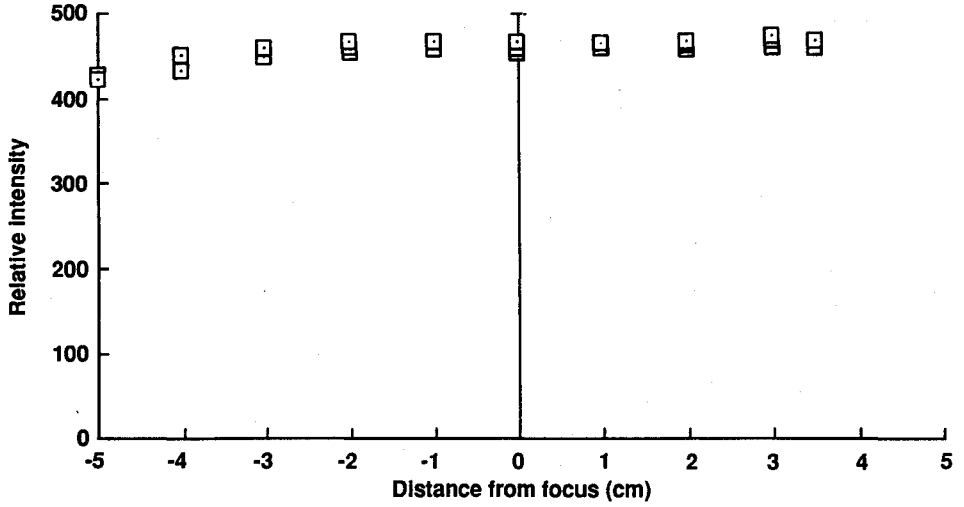

Fig. 4 Relative variation in the intensity at the detector plane as the surface source is moved with respect to the center of the driven tube.

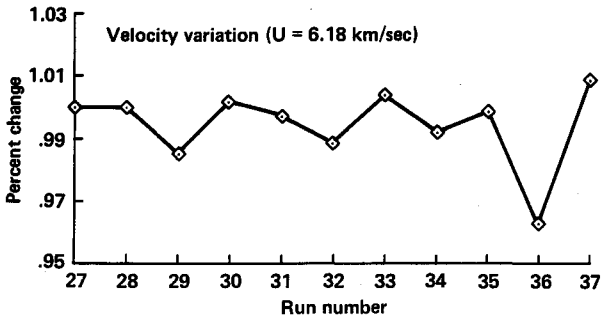

Fig. 5 Run-to-run variation of shock velocity.

than the equilibrium radiation by a factor of 2.5. In addition, one sees stronger radiation from the higher vibrational and rotational levels. Prominently, the increase in radiation in the high vibrational states occurs in the $N_2(2^+)$ bands. The nonequilibrium radiation in the $N_2(2^+)$ system is a factor of 40 higher than the equilibrium region, as compared to the $N_2^+(1^-)$ system, which is only 2.5 times higher than its equilibrium value. In other words, more of the nonequilibrium effect is in the N_2 than in the N_2^+ system. Therefore, $N_2(2^+)$ bands should provide more accurate data on the deviation of vibrational and rotational temperatures from their equilibrium values than N_2^+.

In order to determine the vibrational and rotational temperatures, it was desirable to resolve the vibrational-rotational structure more clearly than was achieved in the runs made with the 0.54 Å per diode-element spectral resolution. By changing the 1200 lines per mm grating to 2400 lines per mm grating, the spectral resolution was improved to 0.3 Å per element. A suitable band system for these measurements was selected on the following criteria: 1) the band system should be isolated, i.e., the radiation measured at that spectral location should be predominantly due to a single band system; 2) at least two vibrational bands, with the rotational structure reasonably resolved, should be visible; and 3) the ratio of nonequilibrium to equilibrium radiation intensities for the band system should be large (see the Appendix). As mentioned earlier, since it was realized that $N_2(2^+)$ band systems would provide more accurate information on the nonequilibrium, our choice was limited to this band system. The (0,1)–(2,1) bands of $N_2(2^+)$ seemed to qualify based on these criteria, and the spectrometer was set to these bands for the next two runs, one for the equilibrium radiation and the other for the nonequilibrium radiation. The improved spectral res-

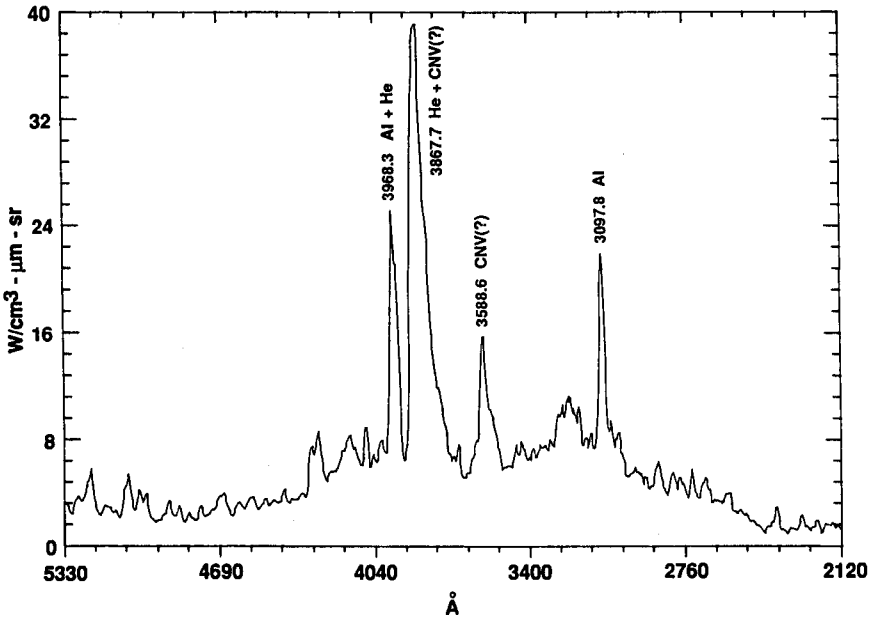

Fig. 6 Emission spectrum of the driver gas.

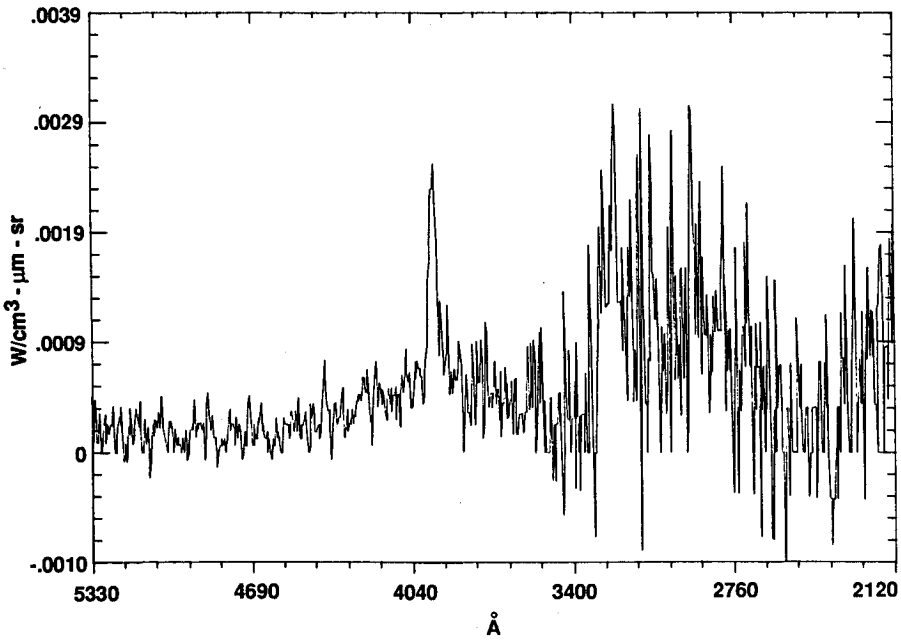

Fig. 7 Emission spectrum recorded 5 μs before the shock arrival: image intensifier gate = 1 μs; shock velocity = 6.79 km/s; spectrometer slit width = 60 μm.

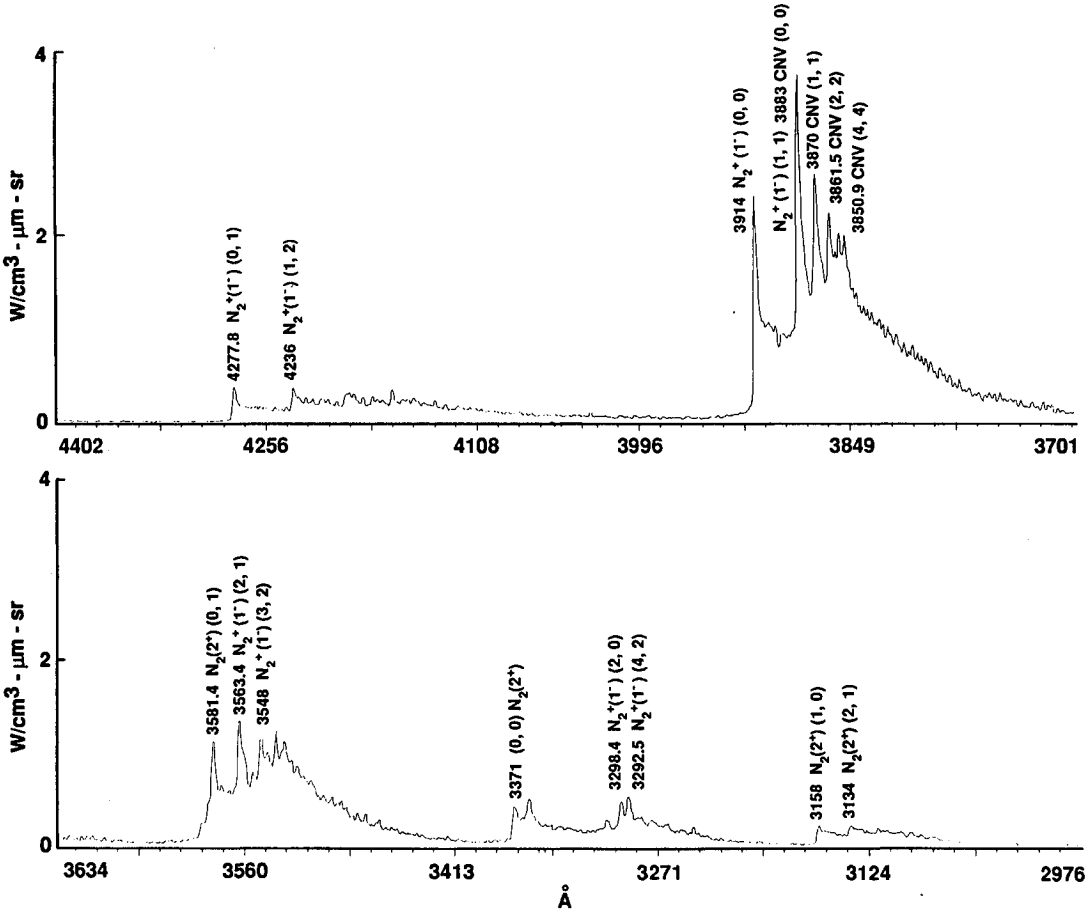

Fig. 8 Equilibrium radiation spectrum: shock velocity = 6.20 km/s; P_1 = 1 Torr in nitrogen; image intensifier gate = 2.5 μs; spectrometer slit width = 60 μm; spectrum resolution = 0.54 Å per diode.

olution can be seen in the equilibrium and nonequilibrium spectra shown in Figs. 10 and 11.

Analysis and Discussion

Conceptually, rotational temperature could be deduced from the ratio of the intensity of one rotational line to that of another. However, this is not practical because the rotational lines overlap and the sensors lack spectral resolution required to discriminate each rotational line. Therefore, the following procedure was adopted in the present work. Using the NEQAIR[11] code, an equilibrium spectrum was first computed by selecting the equilibrium temperature corresponding to the

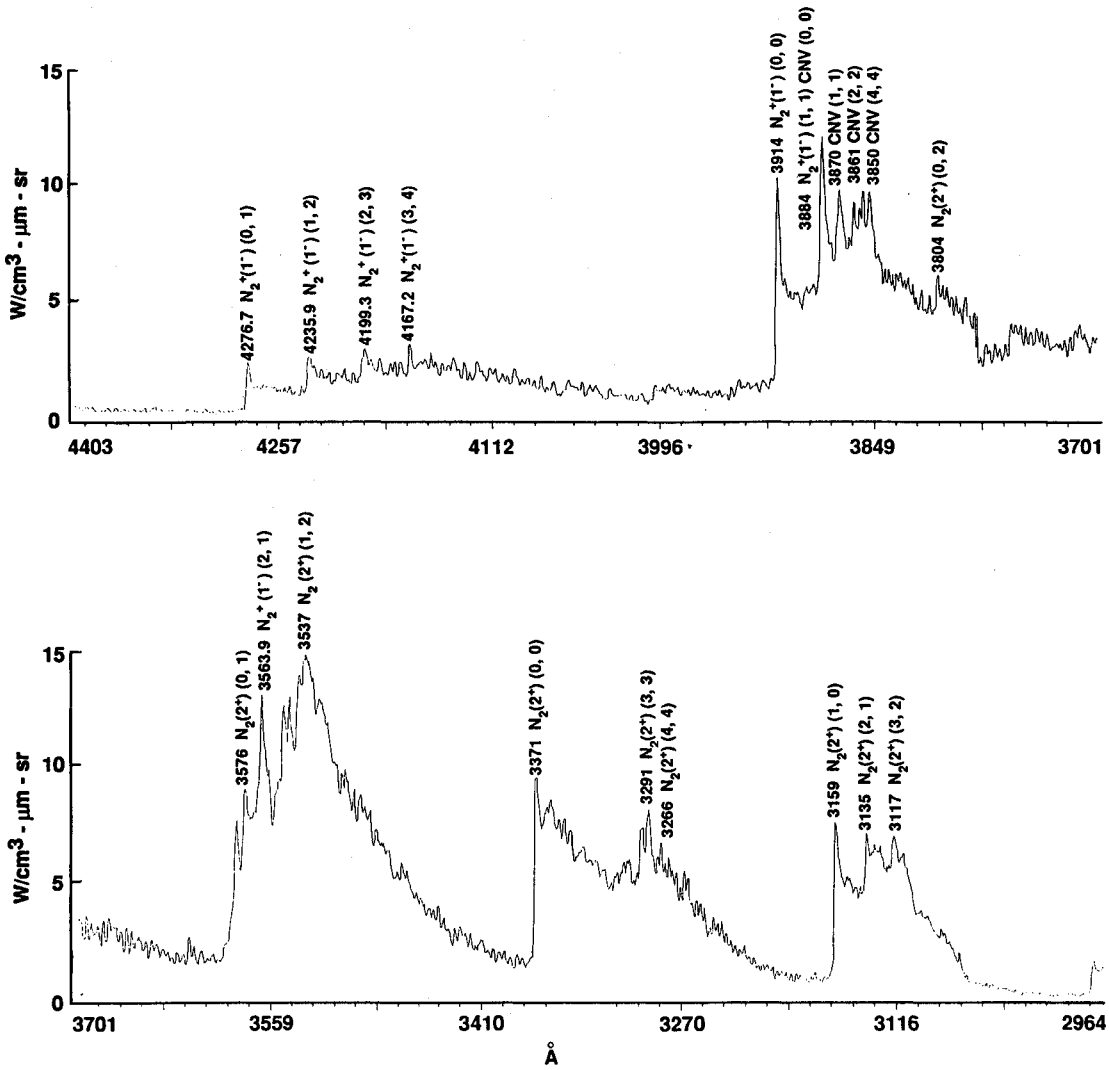

Fig. 9 Nonequilibrium radiation spectrum: shock velocity = 6.20 km/s; P_1 = 1 Torr in nitrogen; image intensifier gate = 200 ns; spectrometer slit width = 60 μm; spectral resolution = 0.54 Å per diode.

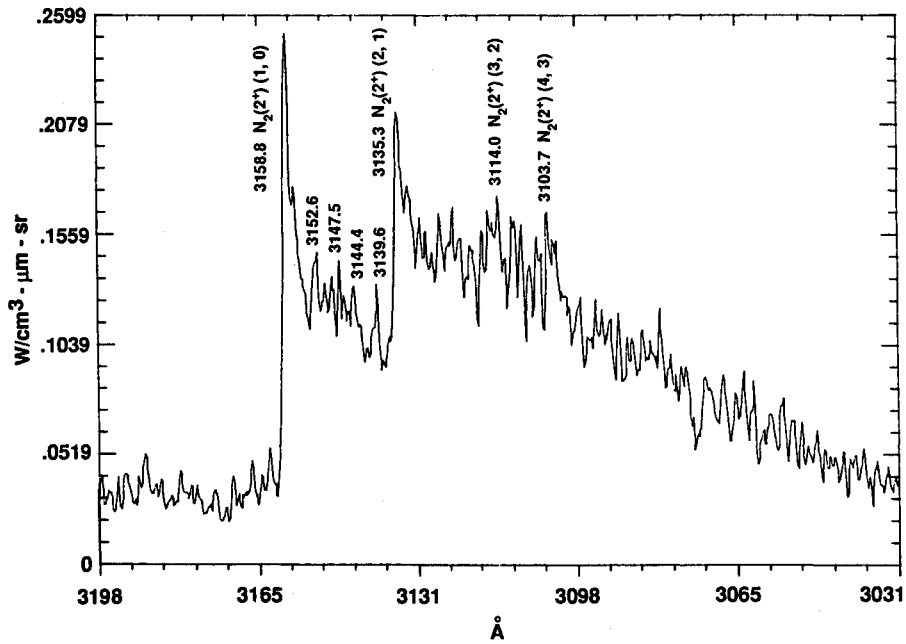

Fig. 10 Equilibrium radiation spectrum: shock velocity = 6.26 km/s; P_1 = 1 Torr in nitrogen; image intensifier gate = 2.5 μs; spectrometer slit = 60 μm; spectral resolution = 0.3 Å per diode.

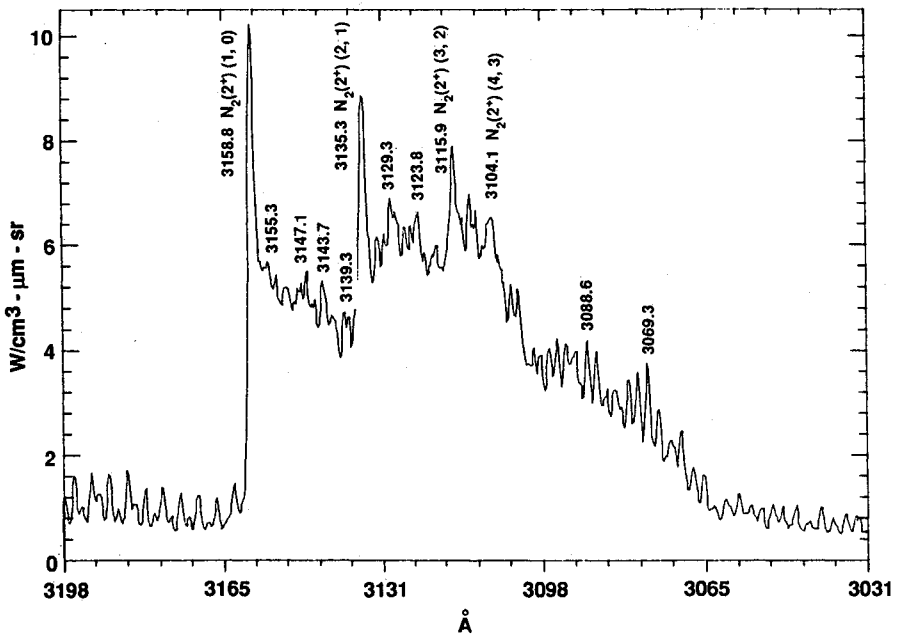

Fig. 11 Nonequilibrium radiation spectrum: shock velocity = 6.26 km/s; P_1 = 1 Torr in nitrogen; image intensifier gate = 200 ns; spectrometer slit = 60 μm; spectral resolution = 0.3 Å per diode.

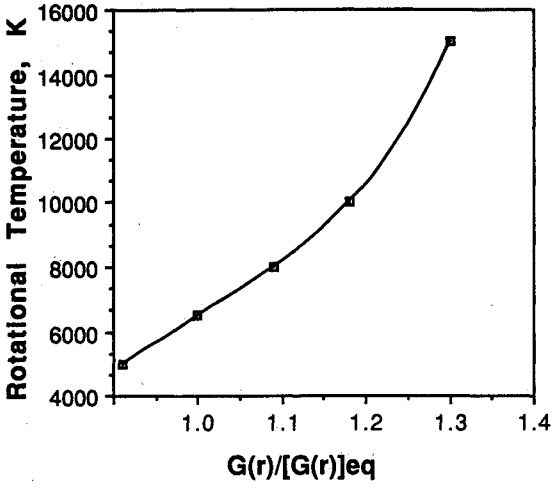

Fig. 12 Function $G(r)/G(r)_{equ}$ as a function of rotational temperature: $T_v = T_e = T_{equ}$ = 6500 K.

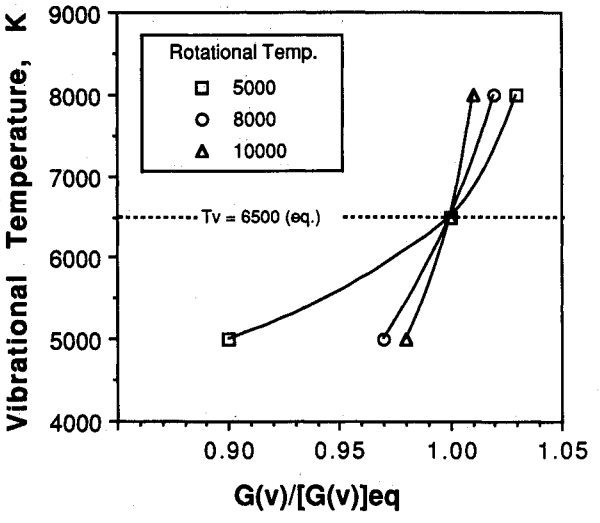

Fig. 13 Function $G(v)/G(v)_{equ}$ as a function of vibrational temperature for various rotational temperatures.

6.20-km/s shock velocity. Only three species were considered: N_2, N_2^+, and e^-. The theoretical spectrum was modified to account for the slit function of the spectrometer and was integrated to compute the output at each diode element using their actual physical dimension (25 μm/element). The equilibrium input temperature was varied until the synthetic spectrum was identical to the measured spectrum. This temperature at which both spectra matched was considered to be the equilibrium temperature of the test gas. The temperature so deduced was 6500 K. The computer code STRAP[7] predicted for this case was approximately 6520 K. The measured temperature of 6500 K and the computed value of 6520 K from STRAP agreed closely with AVCO's measurements.

For a given vibrational band, a function $G(r)_{eq}$ was defined for a given point on the rotational envelop of the equilibrium spectrum as the intensity at that point divided by the peak value of the band system. Then, assuming that the effects of the vibrational temperature on the rotational structure was negligible, several spectra were generated by varying only the rotational temperature while keeping $T_v = T_e = T_{eq}$. Again, the function $G(r)$ for the same given point on the rotational envelop from the nonequilibrium spectrum ($T_R \neq T_{equ}$) was computed as the intensity from this spectrum at that point divided by the peak intensity of band system. Finally, a plot for the given point on the rotational envelop was generated as being a plot of $R(r)/G(r)_{eq}$ as a function of the rotational temperature. Now this plot can be used to compute the rotational temperature from the experimental data, provided $G(r)$ and $R(r)_{eq}$ are available for the corresponding point on the rotational envelop. Ideally, any point on the rotational envelop should provide a useful plot for the determination of the rotational temperature. However, the dependence of $G(r)/G(r)_{eq}$ on the rotational temperature is not uniformly strong for all such points. For the present conditions, the curve shown in Fig. 12 was found to be most sensitive.

A similar procedure was applied for the determination of the vibrational temperature. In this case, a function $G(v)$ was defined as the peak intensity of a higher vibrational band divided by the peak value of a certain lower vibrational band. As in the case of the rotational temperature, $G(v)$ were normalized by their equilibrium values $G(v)_{eq}$ taken from the same two sets of the vibrational bands. The $G(v)$ were obtained by varying the vibrational temperature T_v with $T_e = T_{eq}$. The ratio $G(v)/G(v)_{eq}$ was then plotted as a function of

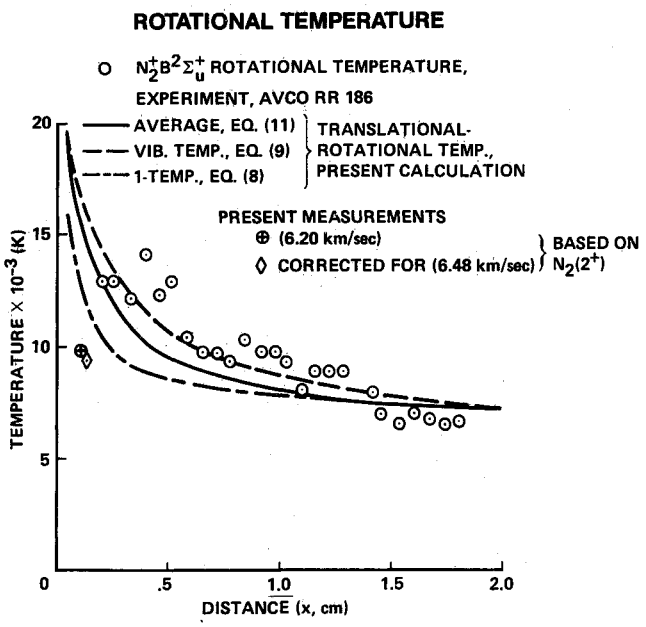

Fig. 14 Measured rotational temperature compared with the AVCO data[3] and with the theoretical values computed by Park[7] using 1) average temperature, 2) vibrational temperature, and 3) translational temperature.

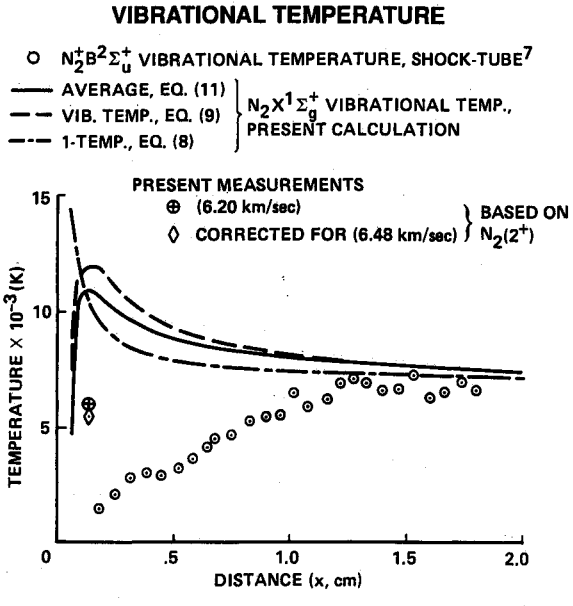

Fig. 15 Measured vibrational temperature compared with the AVCO data[3] and with the theoretical values computed by Park[7] using 1) average temperature, 2) vibrational temperature, and 3) translational temperature.

the vibrational temperature. Several plots were generated for individual rotation temperatures, as shown in Fig. 13. Now that curves in Fig. 13 can be used to determine the vibrational temperature from the experimental data, provided the ratio $G(v)/G(v)_{equ}$ for the same set of the vibrational bands from the experiment, as well as the rotational temperature, is known.

Using the plot in Fig. 12, the rotational temperature in the nonequilibrium region, based on the intensities at 3143.7 and 3159.1 Å, was found to be 8800 ± 203 K (see the Appendix). This temperature is compared with the theoretical computations of Park[7] and the experimental values from the AVCO experiments[3] in Fig. 14. Park used the rate constant parameter K in the following form

$$K = CT^n \exp(-H_0/kT) \quad (1)$$

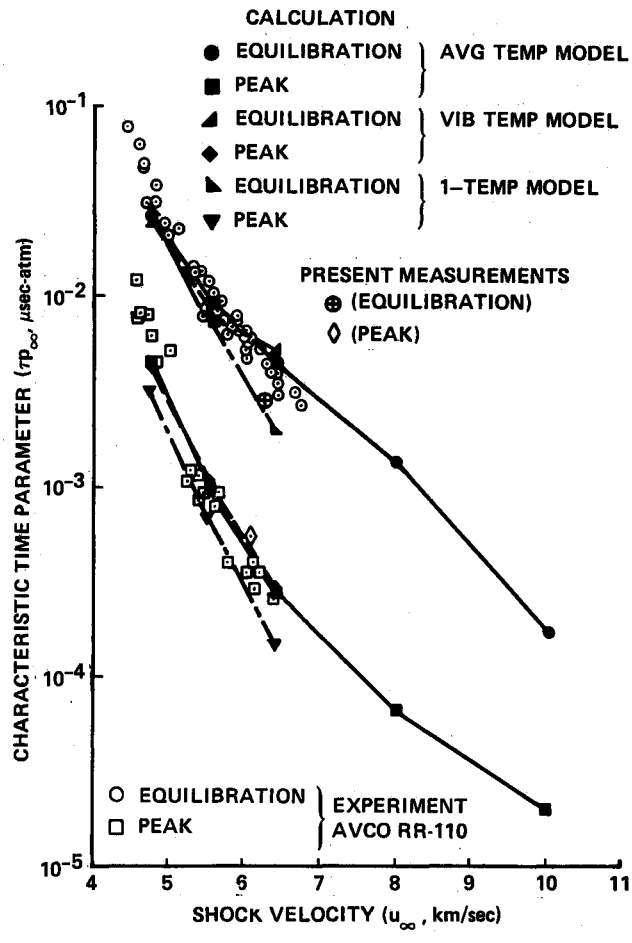

Fig. 16 Measured time required to achieve the peak intensity and the time required to achieve equilibrium compared with the AVCO data[3] and with the theoretical values computed by Park[7] using 1) average temperature, 2) vibrational temperature, and 3) translational temperature.

where C is a constant, n the pre-exponent power index, and H_0 the dissociation energy. For T, three different temperatures were selected for three sets of calculations: 1) the one-temperature model $T = T_v = T_r$ is used in Eq. (1); 2) the vibrational temperature model T_v is used in Eq. (1); and 3) the geometrical average temperature model $T_a = \sqrt{(T \times T_v)}$ is used. Assuming that the rotational and the translational temperatures are the same, three sets of the relaxation calculations are carried and the translational-rotational temperature as a function of the distance is plotted from the three sets in the figure. For these computations, Park assumed that most of the vibrational energy is in the ground electronic state of N_2. Since the present data are for 6.20 km/s, a second point corrected for 6.48 km/s is also plotted in his figure for the purpose of comparison with the AVCO data. The rotational temperature determined in the present experiment is considerably lower than what is expected from the extrapolation of AVCO's data or that predicted by Park. It is true that the rotational temperature measured in this work is based on the $N_2(2^+)$ bands, the theoretical values are based on the ground electronic states of N_2, and the AVCO data are based on N_2^+ bands. However, rotational temperatures are expected to equalize quickly among different molecules and different electronic states. Therefore, the observed discrepancy can not be attributed to this difference. More likely, the true rotational temperature near the shock front is indeed lower, not in equilibrium with the translational temperature. That is, the low rotational temperature observed here is consistent with the AVCO data and merely fills in the missing point in AVCO's data in the initial region of rotational nonequilibrium. Thus,

both the AVCO data and the present data show the fact that rotational temperature is not in equilibrium with the translational temperature, but is relaxing over the observed range. Park's model assumes that the rotational temperature is in equilibrium with the vibrational temperature. The model thus contradicts these experimental data.

The measured vibrational temperature, based on the intensities at 3159.1 and 3135 Å, is found to be 6100 ± 560 K (see the Appendix) and is compared with the theoretical computations of Park[7] and the AVCO data[3] in Fig. 15. The present measurement agrees fairly well with the theoretical prediction by Park, thereby rendering support to Park's model regarding vibrational relaxation. However, compared with AVCO's data, the present result is much higher. This discrepancy could be attributed to the fact that the present measurement is with the $N_2(2^+)$ bands, whereas the AVCO data are for the N_2^+ bands. Vibrational energy transfer between N_2 and N_2^+ is not necessarily fast, and, therefore, one could surmise that these two molecules are at totally different vibrational temperatures.

The characteristic relaxation times, that is, the time to the peak intensity point and the time to equilibrium, determined in the present work are compared with the AVCO data and Park's calculation in Fig. 16. The present data agree with the existing data.

As seen here, the spectral data yield the vibrational and rotational temperatures at one point, or one instant, behind the shock wave. If a two-dimensional diode array is used in place of the linear array used in the present experiment, it will be possible to determine the time history and evolution of the radiation spectra and the rotational and vibrational temperatures in a single run. Such plans are being made at NASA Ames Research Center.

Conclusions

A spectrographic technique incorporating a 700-element linear diode array capable of recording instantaneous radiation has been developed at NASA Ames Research Center for the investigation of radiation characteristics in the thermochemical nonequilibrium region behind a normal shock wave. A spectral resolution of 0.30–0.54-Å per diode element was achieved with this system. A radiation measurement was conducted in the electric-arc driven shock tube. Using the available computer codes, the rotational and vibrational temperatures are deduced from the spectral intensity characteristics of the N_2 second positive system. The rotational temperature was determined to be 6500 K in the equilibrium region, which agreed closely with the data obtained previously by AVCO-Everett Research Laboratory and theoretical calculations carried out using the computer code by Park. However, the vibrational and rotational temperatures of 6100 ± 560 and 8800 ± 230 K obtained in the nonequilibrium region were greatly different from those reported by AVCO. The present rotational temperature data indicate that the rotational mode is in nonequilibrium, thereby invalidating Park's assumption of equilibrium between translational and rotational modes. The present vibrational temperature value agrees with Park's calculation, thereby rendering support to Park's model regarding vibrational relaxation.

Appendix: Error Analysis

For a given function $Q = f(q_1, q_2, q_3, \ldots q_n)$ of independent observations, $q_1, q_2, \ldots q_n$, the standard deviation R can be expressed as

$$R = \sqrt{\left(\frac{\partial Q}{\partial q_1}\right)^2 r_1^2 + \ldots + \left(\frac{\partial Q}{\partial q_n}\right)^2 r_n^2} \qquad \text{(A1)}$$

where $r_1, r_2, \ldots r_n$ are standard deviations for the observations $q_1, q_2, \ldots q_n$, respectively. The function Q can be assumed to be G/G_{eq}, where

$$G = \frac{I_1}{I_2} \qquad \text{(A2)}$$

and I_1 and I_2 are the measured radiation intensities at two given wavelengths, as needed for temperature computations described earlier. G and G_{eq} are the ratios as defined by Eq. (A2) for the nonequilibrium and equilibrium regimes. In general, the quantities I_1 and I_2 are the sums of the actual signal and the instrumental and statistical photoelectron noise. Because of very short integration time (~200 ns), the dark current in the diode array system is negligible and the instrumental noise is limited to the readout noise only (~1.3 counts); the signal noise is approximately equal to the statistical photoelectron noise:

$$\text{noise} = \sqrt{\text{signal}} \qquad \text{(A3)}$$

Then the standard deviation R

$$R = \frac{G}{G_{eq}} \sqrt{\frac{1}{I_1} + \frac{1}{I_2} + \frac{1}{I_1^{eq}} + \frac{1}{I_2^{eq}}} \qquad \text{(A4)}$$

The standard temperature deviation then becomes

$$\sigma_T = \frac{\partial T}{\partial (G/G_{eq})} R \qquad \text{(A5)}$$

where $\partial T/[\partial(G/G_{eq})]$ is determined from the dependence of T on G/G_{eq}.

Acknowledgment

The authors express their gratitude to Chul Park for his valuable guidance and advice throughout this research work.

References

[1]Sharma, S. P., and Park, C., "A Survey of Simulation and Diagnostic Techniques for Hypersonic Nonequilibrium Flows," AIAA Paper 87-0406, Jan. 1987.

[2]Allen, R. A., Keck, J. C., and Camm, J. C. "Non-Equilibrium Radiation from Shock Heated Nitrogen and a Determination of the Recombination Rate," AVCO-Everett Research Laboratory, Everett, MA, Rept. 110, June 1961.

[3]Allen, R. A., "Nonequilibrium Shock Front Rotational, Vibrational and Electronic Temperature Measurements," AVCO-Everett Research Laboratory, Everett, MA, Rept. 186, Aug. 1964.

[4]Allen, R. A. Camm, J. C., and Keck, J. C., "Radiation from Hot Nitrogen," AVCO-Everett Laboratory, Rept. 102, April 1961.

[5]Keck, J. C., Camm, J. C., Kivel, B., and Wentink, T., Jr., "Radiation from Hot Air, Part II," AVCO-Everett Research Laboratory, Everett, MA, Rept. 42, Feb.

[6]Park, C., "Radiation Enhancement by Nonequilibrium in Earth's Atmosphere," *Journal of Spacecraft and Rockets*, Vol. 22, No. 1, 1985, pp. 27–36.

[7]Park, C., "Assessment of a Two-Temperature Kinetic Model for Dissociating and Weakly Ionizing Nitrogen," *Journal of Thermophysics and Heat Transfer*, Vol. 2, No. 1, 1988, pp. 8–16.

[8]Sharma, S., Huo, W. M., and Park, C., "The Rate Parameters for Coupled Vibration-Dissociation in a Generalized SSH Approximation," AIAA Paper 88-2714, July 1988.

[9]Reller, J. O., "Design and Performance of the Ames Electric-Arc Shock Shock Tunnel," NASA TM X-2814, June 1963.

[10]Sharma, S. P., and Park, C., "Operating Characteristics of a 60 cm and a 10 cm Electric Arc Driven Shock Tube," AIAA Paper 88-0142, Jan. 1988.

[11]Park, C., "Nonequilibrium Air Radiation (NEQAIR) Program: User's Manual," NASA TM 86707, July 1985.

[12]Scarborough, J. B., *Numerical Mathematical Analysis*, The Johns Hopkins Press, Baltimore, MD, 1930.